Aquatic Geochemistry (2021) 27:207–220
https://doi.org/10.1007/s10498-021-09396-0

ORIGINAL ARTICLE

The Abiotic Nitrite Oxidation by Ligand-Bound Manganese (III): The Chemical Mechanism

George W. Luther III[1] · Jennifer S. Karolewski[2,3] · Kevin M. Sutherland[4] · Colleen M. Hansel[2] · Scott D. Wankel[2]

Received: 5 April 2021 / Accepted: 18 May 2021 / Published online: 31 May 2021

Abstract

Given their environmental abundances, it has been long hypothesized that geochemical interactions between reactive forms of manganese and nitrogen may play important roles in the cycling of these elements. Indeed, recent studies have begun shedding light on the possible role of soluble, ligand-bound Mn(III) in promoting abiotic transformations under environmentally relevant conditions. Here, using the kinetic data of Karolewski et al. (Geochim Cosmochim Acta 293:365–378, 2021), we provide the chemical mechanism for the abiotic oxidation of nitrite (NO_2^-) by Mn(III)-pyrophosphate, $Mn^{III}PP$, to form nitrate (NO_3^-). Nitrous acid (HNO_2), not NO_2^-, is the reductant in the reaction, based on thermodynamic and kinetic considerations. As soluble Mn(III) complexes react in a one-electron transfer reaction, two one-electron transfer steps must occur. In step one, HNO_2 is first oxidized to nitrogen dioxide, $\cdot NO_2$, a free radical via a hydrogen atom transfer (HAT) reaction. We show that this inner sphere reaction process is the rate-limiting step in the reaction sequence. In step two, $\cdot NO_2$ reacts with a second $Mn^{III}PP$ complex to form the nitronium ion (NO_2^+), which is isoelectronic with CO_2. Unlike the poor electron-accepting capability of CO_2, NO_2^+ is an excellent electron acceptor for both OH^- and H_2O, so NO_2^+ reacts quickly with water to form the end-product NO_3^- (step 3 in the reaction sequence). Thus, water provides the O atom in this nitrification reaction in accordance with the O-isotope data. This work provides mechanistic perspective on a potentially important interaction between Mn and nitrogen species, thereby offering a framework in which to interpret kinetic and isotopic data and to further investigate the relevance of this reaction under environmental conditions.

✉ George W. Luther III
luther@udel.edu

1 School of Marine Science & Policy, University of Delaware, Lewes, DE 19958, USA

2 Department of Marine Chemistry and Geochemistry, Woods Hole Oceanographic Institution, Woods Hole, Falmouth, MA 02540, USA

3 Department of Earth, Atmospheric and Planetary Sciences, Massachusetts Institute of Technology, Cambridge, MA 02139, USA

4 Department of Earth and Planetary Sciences, Harvard University, Cambridge, MA 02138, USA

1 Introduction

Links among various elemental cycles are a hallmark of biogeochemical complexity across Earth's biosphere. Further, biogeochemical interactions between elemental cycles are driven by complex networks of both biological and chemical reactions often operating within close proximity, making it difficult to disentangle their relative roles. For example, while very few reports exist of microorganisms directly coupling energy-gaining redox reactions between manganese (Mn) and nitrogen (N), repeated evidence has emerged from redox gradients in natural sediments for the chemical coupling of Mn reduction to oxidation of N species (e.g., Luther et al 1997; Lin and Taillefert 2014; Anschutz et al. 2000). The work on the chemical mechanism for abiotic Mn/N reactions is limited to the abiotic nitrification reaction of nitrite species with MnO_2 (Luther and Popp 2002) and to the oxidation of NH_2OH to N_2O by MnO_2 (Cavazos et al. 2018). This is in contrast to the work on chemical mechanisms of solid-phase oxidized Mn (e.g., MnO_2) with other reductants, e.g., H_2S (Herzsage and Afonso 2003; Yao and Millero 1993, 1995; Luther et al. 2018), organic compounds (Matocha et al. 2001; Stone and Morgan 1984a, b), and As(III) (Owings et al. 2019). Interestingly, all these studies did not include isotope studies although they discussed electron transfer, intermediates, and molecular mechanisms.

Recently, Karolewski et al. (2021) performed a study on the reaction of Mn(III)-pyrophosphate [$Mn^{III}PP$] with nitrite leading to the formation of nitrate (Eq. 1), an abiotic nitrification reaction.

$$NO_2^- + H_2O + 2Mn^{III}PP \rightarrow 2\,Mn^{II}PP + NO_3^- + 2H^+ \quad (1)$$

The experimental details were well documented, and the results show a rate law as in Eq. 2.

$$\frac{d}{dt}\left[NO_3^-\right] = k\left[Mn^{III}PP\right]^2\left[HNO_2\right]. \quad (2)$$

The reported isotope data also clearly demonstrated that the additional O atom in the product nitrate originated from water, the solvent, as also indicated in Eq. 1. Their nitrogen isotope data exhibited an inverse N isotope effect, which while unusual is consistent with that occurring during microbial nitrite oxidation observed directly in culture studies as well as inferred from field measurements in several oxygen-deficient zones (ODZs) and sediment porewaters (Buchwald and Casciotti 2013; Casciotti, 2009, 2016). Mn(III)–ligand complexes are found in many environmentally relevant redox transition zones, such as ODZs, constituting a substantial fraction of the dissolved Mn pool (Trouwborst et al. 2006; Oldham et al. 2015, 2017a, Delwig et al. 2012). As the kinetics of the various abiotic and biotic nitrite oxidation reactions are similar, oxidized Mn could be at least partly responsible for the conversion of nitrite to nitrate within environmental systems.

The focus of Karolewski et al. (2021) was primarily on regulation of reaction rates and isotope dynamics and did not address possible chemical reaction mechanisms, including electron transfer processes, the formation of any intermediates ($\cdot NO_2$, NO_2^+), and how the O atom comes from water to form NO_3^-. Their rate law suggests that the oxidation of nitrite must occur via two one-electron transfers as Mn(III) can only accept one electron; nevertheless, they did not describe any electron transfers or intermediates. Here, using the recently reported kinetic and isotope data together with thermodynamic data from other works, we provide a more developed description of the redox processes involved, including the specific chemical species that react at different pH values and the steps of reaction

progress that include intermediates. Lastly, we perform an analysis of the molecular structure and molecular orbital properties of the reactants and intermediates to describe chemical mechanisms for each step of the reaction progress.

2 Results

The thermodynamics of the reactions over a range of pH values leads to mechanistic details of the reaction and is described first. We show that there are three steps to the overall reaction, which involves the transformation of HNO_2 to $\cdot NO_2$ to NO_2^+ to the end-product, NO_3^-.

2.1 Two one-electron transfer steps

Because Eq. 1 starts with a complex of Mn(III), HNO_2 or NO_2^- must act as a one-electron transfer reductant. Here, we summarize the relevant reaction progress of two one-electron transfer steps as going from HNO_2 or NO_2^- to $\cdot NO_2$ to NO_3^- using thermodynamics and kinetics. The electron transfer must be inner sphere for Mn as there is a mismatch of symmetry for the highest occupied molecular orbital (HOMO) of HNO_2 or NO_2^- (π^* orbital) and the lowest unoccupied molecular orbital (LUMO) of Mn(III) (σ orbital) (Luther 2005, 2016). The first step in the reaction is likely a hydrogen atom transfer reaction (HAT). Recently, Luther et al. (2018) described HAT reactions for the reduction of MnOOH, MnO_2, and HNO_2 by leucoberbelein blue (LBB). The reaction is pH independent for MnO_2 (a two-electron oxidant) and pH dependent for the one-electron oxidants MnOOH and HNO_2 (Jones et al. 2019; Luther et al. 2018). HAT reactions for LBB are a function of the C–H homolytic bond dissociation energy (BDE) for triphenylmethane compounds that ranges from 293 to 335 kJ mol^{-1} (Zhang and Bordwell 1992). If the thermodynamics of the oxidized Mn reduction half-reactions is more negative than the BDE value, the reaction is favorable. The O–H homolytic bond dissociation energy for HNO_2 is 329 kJ mol^{-1} (Bach et al. 1996), so HNO_2 can react with oxidized Mn in a similar manner to LBB.

2.2 Thermodynamics of the nitrogen species HNO_2, $\cdot NO_2$, and NO_3^- over a range of pH

Oxidation of nitrite to nitrate by soluble Mn(III) compounds occurs via two sequential one-electron transfers according to the stoichiometry in Eq. 1 and can be represented by the following two equations that represent the first (Eqs. 3, 4) and second electron transfer steps (Eq. 5). As shown in the following text and as shown for the reaction of MnO_2 with nitrite (Luther and Popp 2002), oxidation of HNO_2 is thermodynamically favored over NO_2^-. The free radical nitrogen dioxide, $\cdot NO_2$, is the expected metastable intermediate. Equations 3 and 5 demonstrate the pH dependence of the overall reaction as previously reported (Karolewski et al. 2021).

$$HNO_2 \rightarrow \cdot NO_2 + H^+ + e^-. \tag{3}$$

A HAT reaction, which is analogous to Eq. 3, is represented by Eq. 4 (Luther et al. 2018).

$$HNO_2 \rightarrow \cdot NO_2 + H\cdot \quad \text{where } H^+ + e^- = H\cdot \tag{4}$$

$$\cdot NO_2 + H_2O \rightarrow NO_3^- + 2H^+ + e^-. \tag{5}$$

There is also a mismatch of orbital symmetry for $\cdot NO_2$ (the intermediate formed after the loss of the first electron from nitrite) and Mn(III), also indicating that this reaction is an inner sphere electron transfer.

2.3 Thermodynamics of HNO_2 (NO_2^-), $\cdot NO_2$, NO_3^- redox half-reactions and acid dissociation

From Luther (2010, 2016) and Luther and Popp (2002), we have the following acid dissociation (Eq. 6) reaction and redox half-reactions with their thermodynamic functions over pH (Eqs. 7–9).

$$HNO_2 \leftrightarrow NO_2^- + H^+ \text{ (dissociation)} \quad pK_a = 3.25 \tag{6}$$

The redox half-reactions and calculations are at *standard state conditions*, and potentials are given versus the normal hydrogen electrode (NHE). The first electron transfer will be shown to be the rate-limiting step and is a function of pH. We write the redox half-reactions as reduction reactions noting that the reverse (oxidation) half-reactions ('a') are operative for the processes discussed here. The reverse half-reaction, $p\varepsilon_{oxid}$, is Eq. 7a and occurs during $Mn^{III}PP$ reduction (see eqs. 3–5).

$$\cdot NO_2 + H^+ + e^- \rightarrow HNO_2 \quad p\varepsilon_{red} = \log K_{red} = p\varepsilon^o - pH = 16.51 - pH \tag{7}$$

$$p\varepsilon_{oxid} = \log K_{oxid} = -p\varepsilon^o + pH = -16.51 + pH \tag{7a}$$

$$\cdot NO_2 + e^- \rightarrow NO_2^- \quad p\varepsilon_{red} = \log K_{red} = p\varepsilon^o = 15.60 \tag{8}$$

$$p\varepsilon_{oxid} = \log K_{oxid} = -15.60. \tag{8a}$$

The half-reaction for the reduction of NO_3^- to $\cdot NO_2$ (the second electron transfer step) is Eq. 9.

$$NO_3^- + 2H^+ + e^- \rightarrow \cdot NO_2 + H_2O \quad p\varepsilon_{red} = \log K_{red} = p\varepsilon^o - 2pH = 13.07 - 2\,pH \tag{9}$$

$$p\varepsilon_{oxid} = \log K_{oxid} = 2pH - 13.07. \tag{9a}$$

2.4 Thermodynamics of the Mn^{III}pyrophosphate, $Mn^{III}PP$, reduction half-reaction

The general equation for the first electron transfer of HNO_2, which will be shown to be rate limiting, is given in Eq. 10. Equation 10a using NO_2^- as reductant will be shown to be unfavorable.

$$Mn^{III}PP + HNO_2 \rightarrow Mn^{II}PP + \cdot NO_2 + H^+ \tag{10}$$

$$Mn^{III}PP + NO_2^- \rightarrow Mn^{II}PP + \cdot NO_2. \quad (10a)$$

The second electron transfer is given by Eq. 11 (11a).

$$Mn^{III}PP + \cdot NO_2 + H_2O \rightarrow Mn^{II}PP + NO_3^- + 2H^+ \quad (11)$$

Or

$$Mn^{III}PP + \cdot NO_2 + OH^- \rightarrow Mn^{II}PP + NO_3^- + H^+. \quad (11a)$$

To calculate thermodynamic favorability of these reactions requires data on the reduction of $Mn^{III}PP$ to $Mn^{II}PP$ (Eq. 12).

$$Mn^{III}PP + e^- \rightarrow Mn^{II}PP. \quad (12)$$

Watters and Kolthoff (1948, see their Table 3) measured Mn(III) reduction potentials versus the saturated calomel electrode (SCE) for $Mn^{III}PP$ species (column 3 of Table 1) over the pH range from 0.05 to 8.72. In their work, total concentrations of Mn(III) and Mn(II) were 5 mM, and the total concentration of pyrophosphate was 0.4 M at each pH. Their SCE potentials were converted to potentials versus NHE (column 4 of Table 1) from which the equilibrium constant, K_{red}, and $p\varepsilon_{red}$ (column 5 of Table 1) of the half-reaction could be calculated.

Watters and Kolthoff (1948) also provided information on the protonation of the pyrophosphate ligand over pH. At pH < 3, the complex is $[Mn^{III}(H_2P_2O_7)_3]^{3-}$, and above pH 6, it is $[Mn^{III}(HP_2O_7)_3]^{9-}$ as several H^+ are lost on increasing pH. Thus, both $Mn^{III}PP$ and nitrite speciation vary with pH, and both species will lose H^+ as pH increases (Fig. 1).

The thermodynamics for the reactions represented by Eqs. 10 and 11 can now be calculated to predict the favorability of the reaction over a range of pH values. The thermodynamics of Eq. 10 (column 6 in Table 1) is calculated from the sum of Eq. 7a (column 2 in Table 1) and Eq. 12 (column 5 in Table 1), which is Eq. 13.

$$\Delta \log K_{reaction} = p\varepsilon_{red}\left(Mn^{III}PP\right) + p\varepsilon_{oxid}\left(HNO_2\right) \quad (13)$$

$$\Delta \log K_{reaction} = p\varepsilon_{red}(Mn^{III}PP) + p\varepsilon_{oxid}\left(NO_2^-\right). \quad (13a)$$

Column 6 in Table 1 shows that the reaction (from eqs. 10, 13) is favorable ($\Delta \log K_{reaction} > 0$) at pH values < ~4.3 (Fig. 1).

The first electron transfer using NO_2^- (column 7 in Table 1) rather than HNO_2 shows that NO_2^- is not as favorable as an oxidant for $Mn^{III}PP$ (last column of Table 1; Eq. 10a) as HNO_2. Here, $\Delta \log K_{reaction}$ data (addition of columns 5 and 7; Eq. 13a) indicate that the reaction of $Mn^{III}PP$ with NO_2^- to form $\cdot NO_2$ is favorable only at low pH (<2.3), where NO_2^- is not the dominant chemical species according to Eq. 6 (see also Sect. 3.2). Thus, NO_2^- is not the reductant for $Mn^{III}PP$. These data parallel the thermodynamic data found for the two-electron reduction of MnO_2 by HNO_2 to form NO_3^- (Luther and Popp 2002) where the nitrate formation reaction rate also decreased with increasing pH.

Similarly, the thermodynamic favorability of Eq. 11 is calculated from the sum of Eq. 9a (column 2 in Table 2) and Eq. 12 (column 3 in Table 2), which is Eq. 14.

$$\Delta \log K_{reaction} = p\varepsilon_{red}(Mn^{III}PP) + p\varepsilon_{oxid}(\cdot NO_2). \quad (14)$$

Table 1 Prediction of thermodynamic favorability for the reaction $Mn^{III}PP + HNO_2 \rightarrow Mn^{II}PP + \cdot NO_2 + H^+$ (column 6, Eq. 10) and $Mn^{III}PP + NO_2^- \rightarrow Mn^{II}PP + \cdot NO_2$ (column 8, Eq. 10a)

(1) pH	(2) $p\varepsilon_{oxid} = \log K_{oxid}$ for 1st Electron transfer $HNO_2 \rightarrow \cdot NO_2$ (Eq. 7a)	(3) E (volt) vs SCE $Mn^{III}PP \rightarrow Mn^{II}PP$	(4) E (volt) vs NHE $Mn^{III}PP \rightarrow Mn^{II}PP$	(5) $p\varepsilon_{red} = \log K_{red}$ $Mn^{III}PP \rightarrow Mn^{II}PP$	(6) $\Delta\log K_{reaction} = p\varepsilon_{red} + p\varepsilon_{oxid}$ for $Mn^{(III)}PP$ reduction/ HNO_2 oxidation	(7) $p\varepsilon_{oxid} = \log K_{oxid}$ for 1st electron Transfer $NO_2^- \rightarrow \cdot NO_2$	(8) $\Delta\log K_{reaction} = p\varepsilon_{red} + p\varepsilon oxid$ for $Mn^{III}PP$ reduction/ NO_2^- oxidation
0.05	− 16.46	0.9462	1.187	20.13	**3.67**	15.60	**4.53**
0.19	− 16.32	0.9345	1.176	19.93	**3.61**	15.60	**4.33**
0.52	− 15.99	0.9035	1.145	19.40	**3.41**	15.60	**3.80**
0.8	− 15.71	0.8796	1.121	19.00	**3.29**	15.60	**3.40**
1.12	− 15.39	0.8610	1.102	18.68	**3.29**	15.60	**3.08**
1.52	− 14.99	0.8260	1.067	18.09	**3.10**	15.60	**2.49**
1.76	− 14.75	0.8124	1.054	17.86	**3.11**	15.60	**2.26**
1.97	− 14.54	0.7887	1.030	17.46	**2.92**	15.60	**1.86**
2.27	− 14.24	0.7584	0.9996	16.94	**2.70**	15.60	**1.34**
2.99	− 13.52	0.6680	0.9092	15.41	**1.89**	15.60	*− 0.19*
3.59	− 12.92	0.5780	0.8192	13.88	**0.96**	15.60	*− 1.72*
4.02	− 12.49	0.5185	0.7597	12.88	**0.39**	15.60	*− 2.72*
4.54	− 11.97	0.4282	0.6694	11.35	*− 0.62*	15.60	*− 4.25*
5.85	− 10.66	0.3184	0.5596	9.48	*− 1.18*	15.60	*− 6.12*
7.11	− 9.40	0.2623	0.5035	8.53	*− 0.87*	15.60	*− 7.07*
8.72	− 7.79	0.1870	0.4282	7.26	*− 0.53*	15.60	*− 8.34*

Values of $\Delta\log K_{reaction}$ (columns 6 and 8) that are positive and in bold font indicate a favorable reaction, whereas values in italic font indicate an unfavorable reaction

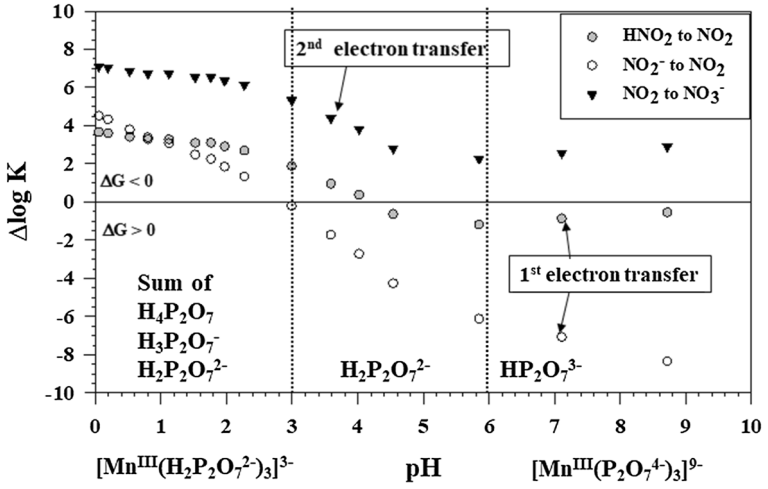

Fig. 1 Thermodynamics of $Mn^{III}PP$ reduction over pH by nitrite species and nitrogen dioxide. The vertical lines indicate the predominant pyrophosphate species noted by Watters and Kolthoff (1948). They also indicate the change in $Mn^{III}PP$ speciation with increasing pH as H^+ dissociates from the pyrophosphate species

Table 2 Prediction of thermodynamic favorability for the reaction $Mn^{III}PP + \cdot NO_2 + H_2O \rightarrow Mn^{II}PP + NO_3^- + 2\ H^+$ (Column 4, Eq. 11)

(1) pH	(2) $p\varepsilon_{oxid} = \log K_{oxid}$ for 2nd electron transfer $\cdot NO_2 \rightarrow NO_3^-$	(3) $p\varepsilon_{red} = \log K_{red}$ $Mn^{III}PP \rightarrow Mn^{II}PP$	(4) $\Delta\log K_{reaction} = p\varepsilon_{red} + p\varepsilon_{oxid}$ for $Mn^{III}PP$ reduction/$\cdot NO_2$ oxidation
0.05	− 13.02	20.13	**7.11**
0.19	− 12.88	19.93	**7.05**
0.52	− 12.55	19.40	**6.85**
0.8	− 12.27	19.00	**6.73**
1.12	− 11.95	18.68	**6.73**
1.52	− 11.55	18.09	**6.54**
1.76	− 11.31	17.86	**6.55**
1.97	− 11.10	17.46	**6.36**
2.27	− 10.80	16.94	**6.14**
2.99	− 10.08	15.41	**5.33**
3.59	− 9.48	13.88	**4.40**
4.02	− 9.05	12.88	**3.83**
4.54	− 8.53	11.35	**2.82**
5.85	− 7.22	9.48	**2.26**
7.11	− 5.96	8.53	**2.57**
8.72	− 4.35	7.26	**2.91**

Values of $\Delta\log K_{reaction}$ that are positive and in bold font indicate a favorable reaction

The fourth column in Table 2 shows that the reaction is favorable ($\Delta\log K_{reaction} > 0$) at pH values up to 8.72 (Fig. 1). Thus, the reaction of $Mn^{III}PP$ with $\cdot NO_2$ to NO_3^- is favorable over all pH conditions considered.

3 Discussion

3.1 Concentration Dependence of HNO_2 as the Reductant

The $\Delta \log K_{reaction}$ values in columns 6 (Eq. 10) and 8 (Eq. 10a) of Table 1 and in column 4 (Eq. 11) of Table 2 are plotted versus pH in Fig. 1. These data again demonstrate that HNO_2 is the reactant and not NO_2^-. The first electron transfer reaction with HNO_2 as the reductant is favorable up to a pH of 4.3 and then becomes slightly inhibited due to thermodynamics. Thus, this is the rate-determining step in the reaction of HNO_2 with $Mn^{III}PP$ to form NO_3^-. The second electron transfer reaction with $\cdot NO_2$ as the reductant has no thermodynamic barrier at these pH values. Thus, this step is likely fast and not rate inhibiting. It is at this point that O atoms from water are added to form nitrate.

The thermodynamic functions 7 and 7a can be expanded as in Eqs. 15 and 15a to include the concentrations of HNO_2 and $\cdot NO_2$. Because $\cdot NO_2$ is a free radical and its reaction with $Mn^{III}PP$ is favorable over all pH values considered, it likely quickly reacts. The $\cdot NO_2$ concentration does not buildup so is negligible at any time point; thus, Eq. 15b is the relevant half-reaction for calculation of thermodynamic favorability.

$$p\varepsilon_{red} = \log K_{red} = p\varepsilon^o - pH = 16.51 - pH + \log[HNO_2] - \log[\cdot NO_2] \quad (15)$$

$$p\varepsilon_{oxid} = \log K_{oxid} = -p\varepsilon^o + pH = -16.51 + pH - \log [HNO_2] + \log[\cdot NO_2] \quad (15a)$$

$$p\varepsilon_{oxid} = -p\varepsilon^o + pH = -16.51 + pH - \log[HNO_2]. \quad (15b)$$

At pH 7.11 and a total nitrite concentration of 100 µM as done in the work of Karolewski et al. (2021), αHNO_2 (i.e., the fraction of nitrite existing in the protonated form) is 1.41×10^{-4}, so $[HNO_2]$ equals 1.41×10^{-8} M (or 14.1 nM). From the following calculations (note that the measured $p\varepsilon_{red}$ includes Mn concentrations), the reaction is thermodynamically favorable at the conditions of the experiments in Karolewski et al. (2021), but slow due to the trace concentration of HNO_2.

$$p\varepsilon_{oxid}(HNO_2) = -16.51 + 7.11 - (-7.85) = -1.56$$

$$p\varepsilon_{red}(Mn^{III}PP) = 8.53$$

$$\Delta \log K_{reaction} = p\varepsilon_{oxid} + p\varepsilon_{red} = 6.7.$$

The vertical lines in Fig. 1 indicate the predominant pyrophosphate species noted by Watters and Kolthoff (1948). They also indicated the change in $Mn^{III}PP$ speciation with increasing pH as H^+ dissociates from the pyrophosphate species. They indicated that the solution color changes from intense violet at pH < 3 where $[Mn^{III}(H_2P_2O_7^{2-})_3]^{3-}$ dominates speciation to less intense violet above pH 3. The solution color changes to amber starting at pH 4.5 and brown-amber as the pH approaches 7, where $[Mn^{III}(P_2O_7^{4-})_3]^{9-}$ dominates speciation. These color changes are consistent with stronger metal–ligand bonding and ligand to metal charge transfer transitions (Luther 2016). Stronger metal–ligand bonding with increased pH also results in less positive or more negative redox potentials (see data in column 3, Table 1), which make the HNO_2 reaction less favorable as observed. In alkaline solutions of pH > 9, OH^- attacks $[Mn^{III}(P_2O_7^{4-})_3]^{9-}$ and leads to the disproportionation of

the $Mn^{III}PP$ complex to Mn(II) and MnO_2 (Klewicki and Morgan 1998; Qian et al 2019; Watters and Kolthoff 1948). At low pH and in the presence of excess pyrophosphate to Mn as done by Karolewski et al. (2021), the complexes are stable to disproportionation (Klewicki and Morgan 1998).

3.2 Kinetics data compared with the concentration of HNO_2 over pH

Figure 2a shows the HNO_2/NO_2^- species diagram over pH and indicates that there is still a minor amount of HNO_2 at higher pH for reaction with $Mn^{III}PP$. Karolewski et al. (2021) documented a slow reaction at pH > 7. In fact, the nitrite oxidation rate data from Table 2 in Karolewski et al. (2021) follow the speciation of HNO_2 not NO_2^-. Here, Fig. 2a, inset, b documents that as the fraction of HNO_2 decreases in solution, the nitrite oxidation rate decreases. Figure 2a shows similar curves for the fraction of species and

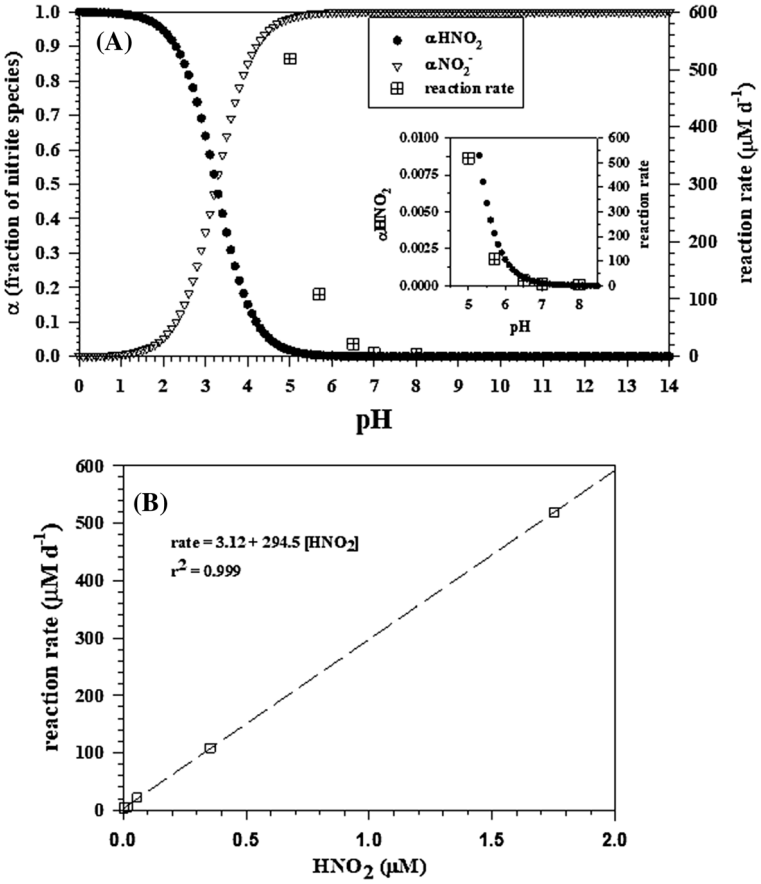

Fig. 2 A) Nitrite species diagram versus pH. The inset shows that the nitrite oxidation rate [taken from Table 2 in Karolewski et al. (2021)] increases with the fraction (concentration) of HNO_2 (αHNO_2). B) Nitrite oxidation rate increases linearly with [HNO_2] (calculated by multiplying αHNO_2 by the concentration of nitrite of 100 μM used in Karolewski et al. 2021)

reaction rates reported in Luther and Popp (2002) and Luther et al. (2018) for the two-electron transfer between HNO_2 and MnO_2; however, that mechanism was postulated to be a O atom transfer from MnO_2 to HNO_2.

3.3 Chemical mechanism for the nitrite to nitrate transformation

Here, we use the Lewis structures for HNO_2, $\cdot NO_2$, NO_2^+ and NO_3^- to describe the complete oxidation of HNO_2 to NO_3^-. Equations 3 and 5 describe the oxidation of HNO_2 to $\cdot NO_2$ to NO_3^-. However, we also note that there is a short-lived intermediate that forms, but which is not represented in these equations. Figure 3 shows two schemes for the complete oxidation and transformation of NO_2^- to NO_3^-. Scheme 1 shows the conversion of HNO_2 to $\cdot NO_2$ via a one-electron transfer. The one-electron oxidation of $\cdot NO_2$ leads to formation of the intermediate NO_2^+, which is isoelectronic with CO_2. Just as CO_2 can react with H_2O and OH^- to form H_2CO_3/HCO_3^-, NO_2^+ reacts with H_2O and OH^- to form HNO_3/NO_3^- as in Scheme 2 of Fig. 3 (Eqs. 16, 16a). Thus, the O atom comes from water in a Lewis acid–base reaction as found with the O-isotope data from Karolewski et al. (2021). Note that loss of H^+ from H_2O increases on oxidation of HNO_2.

$$NO_2^+ + OH^- \rightarrow HNO_3 \rightarrow NO_3^- + H^+ \tag{16}$$

$$NO_2^+ + H_2O \rightarrow HNO_3 + H^+ \rightarrow NO_3^- + 2H^+. \tag{16a}$$

Overall, the N species reaction pathway is from HNO_2 to $\cdot NO_2$ to NO_2^+ to NO_3^-.

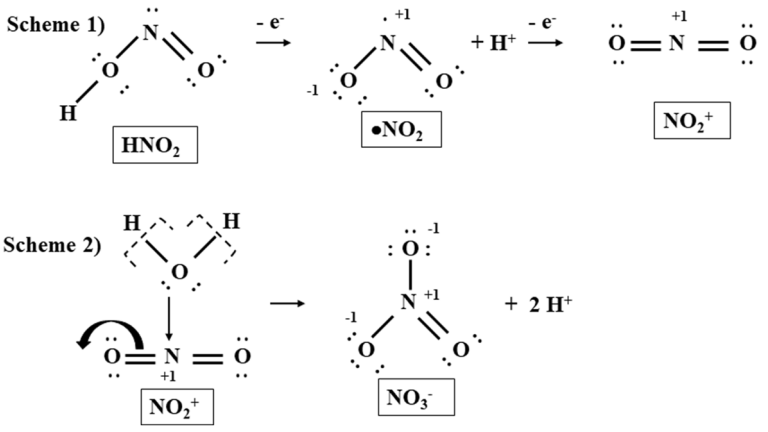

Fig. 3 Lewis structures including formal charges on each atom showing the conversion of NO_2^- to $\cdot NO_2$ to NO_2^+ in Scheme 1. Scheme 2 shows that a bond between the O atom in H_2O forms with the N in NO_2^+; the dashed brackets indicate the electrons from the H–O bonds in H_2O remain with the O atom when H^+ dissociates, and the curved arrow indicates one of the pairs of electrons in the O=N double bond moves to the O atom so NO_3^- results

3.4 Energetics and reactivity of NO_2^+ as a transient intermediate

Unlike the slow kinetics at low pH for the reaction of CO_2 with H_2O to form H_2CO_3, the reaction of NO_2^+ with H_2O is fast enough to promote nitrate formation at low pH. Figure 4 shows the energies of the HOMO and LUMO orbitals (tabulated in Luther 2016) for the relevant species described in this paper. The LUMO energy for NO_2^+ is equivalent to the reverse of the ionization potential of $\cdot NO_2$ (experimental value is 9.75 eV), so the LUMO value is − 9.75 eV. Thus, NO_2^+, which has a positive N atom, is an excellent electron acceptor in contrast to CO_2, which has a LUMO experimental value of + 0.5 eV, indicating it is a poor electron acceptor (Luther 2004). Although the H_2O HOMO energy is − 12.61 eV, this difference of 2.86 eV between the E_{HOMO} of H_2O and the E_{LUMO} of NO_2^+ is an acceptable uphill energy of activation, E_a (Luther 2016). This uphill E_a is similar to that found for the reaction of OH^- with CO_2 (2.325 eV) to form HCO_3^-. In contrast, the OH^- HOMO of − 1.825 eV gives a downhill reaction with NO_2^+ and an energy difference of − 7.925 eV; thus, there is no E_a.

Also, the species OH^-, H_2O, HNO_2, and NO_2^- have HOMO energies that permit the ease of donation of a pair of electrons to a labile Mn(III) complex or a vacant coordination site to form a Mn–O bond. Thus, an inner sphere complex can form prior to electron transfer, which is required for the orbital symmetry mismatch for the HOMO of HNO_2 and the LUMO of Mn(III). The LUMO energies for most transition metals that are labile are more negative than − 14 to − 15 eV so are excellent electron acceptors (Luther 2016). For Mn(III) complexes with a d^4 or $t_{2g}^3e_g^1$ electron configuration for octahedral complexes, Jahn–Teller distortion occurs, which leads to labile complexes and attack of Mn(III) by an electron pair donor (ligand). Here, because of distortion, one O atom from a pyrophosphate ligand can dissociate from Mn(III) for HNO_2 to attack. At alkaline pH, hydroxide ion, which is increased in concentration and is a

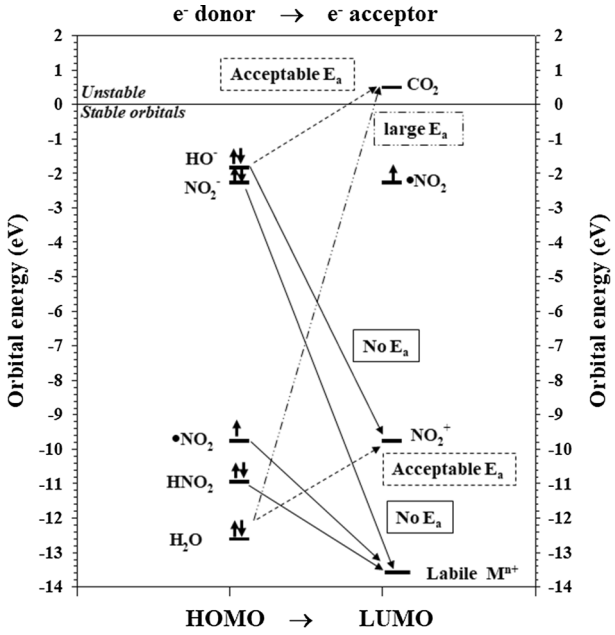

Fig. 4 Energies for the HOMO and LUMO orbitals of the various reactants. The HNO_2 data point is from Hoener et al. (2021). Good electron donors have more positive E_{HOMO} values, whereas good electron acceptors have more negative E_{LUMO} values

stronger nucleophile than the N species in Fig. 4, outcompetes the N species for the Mn in $Mn^{III}PP$. Thus, disproportionation of $Mn^{III}PP$ occurs yielding Mn(II) and MnO_2.

4 Conclusions

Using the kinetic and isotope data from Karolewski et al. (2021) as well as known thermodynamic data for the speciation of the reactants, we show that HNO_2 is the reactant with $Mn^{III}PP$ to form NO_3^-. Using the molecular properties of the intermediate N species ($\cdot NO_2$ and NO_2^+), we show that the O atom must come from H_2O in agreement with the isotope data. The first intermediate formed is $\cdot NO_2$, which on losing an electron to reduce $Mn^{III}PP$ forms NO_2^+, which in turn reacts with H_2O to form NO_3^-.

The investigation of reactions of Mn(III) complexes for environmental applications has been few. Despite the favorable thermodynamic conditions for reactions coupling Mn and N transformations, direct evidence for the occurrence of these reactions in natural systems remains limited. Prior to this study, only two laboratory studies detailed the kinetics of Mn and N reactions and provided mechanistic insight (Cavazos et al. 2018; Luther and Popp 2002). However, the products of some Mn and N reactions have been more widely examined. For reactions with reduced nitrogen compounds, Luther et al. (1997) reacted a Mn^{III}bistris complex with ammonia, NH_3, and found reduction of Mn(III) to Mn(II). In that work, the reaction of a Mn^{III}bistris complex with hydrazine, N_2H_4, also led to N_2. Luther et al. (2018) documented that ammonia, NH_3, (not NH_4^+) oxidation by soluble Mn(III) and MnO_2 are examples of HAT reactions, as proposed here for Mn(III) oxidation of HNO_2. Similarly, the reaction of oxidized Mn with hydroxylamine (NH_2OH), an intermediate in NH_3 oxidation, to form N_2O (Liu et al. 2017; Heil et al. 2016; Zhu-Barker et al. 2015; Cavazos et al. 2018) likely occurs by HAT reactions.

As dissolved Mn(III) complexes can be abundant in a wide range of environments (e.g., Dellwig et al. 2012; Madison et al. 2013; Oldham et al. 2017b, c; Trouwborst et al. 2006; Yakushev et al. 2007), they have the potential to serve as an important control on the redox landscape of natural systems. Beyond nitrogen species, Mn(III) complexes can also oxidize ferrous iron and sulfide (Kostka et al. 1995; Oldham et al. 2015; Siebecker et al. 2015; Trouwborst et al. 2006). In fact, due to the versatility of Mn(III) as both a reductant and oxidant, its presence in the suboxic zone has been implicated in preserving suboxic zones by "titrating" downward diffusing oxygen and upward diffusing reductants (Dellwig et al. 2010; Madison et al. 2013; Trouwborst et al. 2003; Yakushev et al. 2007). We recommend coupling molecular information with more detailed kinetics and isotope experiments exploring oxidized Mn [including dissolved Mn(III)]-mediated reactions, which would permit a more refined assessment of the underlying chemical mechanisms at play and the overall importance of these reactions in sediments, soils, and oxic–anoxic transition zones.

Acknowledgements This work was supported by NSF Geobiology and Low-Temperature Geochemistry grant EAR1826940 to SDW and CMH, by NASA Earth and Space Science Fellowship NNX15AR62H and Agouron Institute Geobiology Postdoctoral Fellowship to KMS, and by NSF Chemical Oceanography grant OCE-1558738 to GWL. All original rate and isotope data can be found at https://doi.org/10.1016/j.gca.2020.11.004. We thank the anonymous reviewers for their constructive comments.

Ethical Approval The authors declare that they have no known competing financial interests or personal relationships that could have appeared to influence the work reported in this paper.

References

Anschutz P, Sundby B, Lefrancois L, Luther GW III, Mucci A (2000) Interactions between metal oxides and species of nitrogen and iodine in bioturbated marine sediments. Geochim Cosmochim Acta 64:2751–2763. https://doi.org/10.1016/S0016-7037(00)00400-2

Bach RD, Ayala PY, Schlegel HB (1996) A reassessment of the bond dissociation energies of peroxides. an ab initio study. J Amer Chem Soc 118:12758–12765. https://doi.org/10.1021/ja961838i

Buchwald C, Casciotti KL (2013) Isotopic ratios of nitrite as tracers of the sources and age of oceanic nitrite. Nat Geosci 6:309–313. https://doi.org/10.1038/ngeo1745

Casciotti KL (2009) Inverse kinetic isotope fractionation during bacterial nitrite oxidation. Geochim Cosmochim Acta 73:2061–2076. https://doi.org/10.1016/j.gca.2008.12.022

Casciotti KL (2016) Nitrite isotopes as tracers of marine N cycle processes. Philosl Trans A 374:20150295. https://doi.org/10.1098/20150295

Cavazos AR, Taillefert M, Tang Y, Glass JB (2018) Kinetics of nitrous oxide production from hydroxylamine oxidation by birnessite in seawater. Mar Chem 202:49–57. https://doi.org/10.1016/j.marchem.2018.03.002

Dellwig O, Leipe T, Marz C, Glockzin M, Pollehne F, Schnetger B, Yakushev E, Bottcher ME, Brumsack HJ (2010) A new particulate Mn–Fe–P-shuttle at the redoxcline of anoxic basins. Geochim Cosmochim Acta 74:7100–7115

Dellwig O, Schnetger B, Brumsack HJ, Grossart HP, Umlauf L (2012) Dissolved reactive manganese at pelagic redoxclines (part II): hydrodynamic conditions for accumulation. J Mar Systems 90(1):31–41. https://doi.org/10.1016/j.jmarsys.2011.08.007

Jannis H, Shurong L, Vereecken H, Brüggemann N 2015) Abiotic nitrous oxide production from hydroxylamine in soils and their dependence on soil properties. Soil Biology and Biochemistry 84:107–115. https://doi.org/10.1016/j.soilbio.2015.02.022

Herszage J, dos Santos AM (2003) Mechanism of hydrogen sulfide oxidation by manganese(IV) oxide in aqueous solutions. Langmuir 19:9684–9692

Hoener M, Bodi A, Hemberger P, Endres T, Kaspe T (2021) Threshold photoionization shows no sign of nitryl hydride in methane oxidation with nitric oxide. Phys Chem Chem Phys 23:1265–1272. https://doi.org/10.1039/d0cp04924g

Jones MR, Luther GW, Mucci A, Tebo BM (2019) Concentrations of reactive Mn(III)-L and MnO_2 in estuarine and marine waters determined using spectrophotometry and the leuco base, leucoberbelin blue. Talanta 200:91–99. https://doi.org/10.1016/j.talanta.2019.03.026

Karolewski JS, Sutherland K, Hansel CM, Wankel SW (2021) An isotopic study of abiotic nitrite oxidation by ligand-bound manganese (III). Geochim Cosmochim Acta 293:365–378. https://doi.org/10.1016/j.gca.2020.11.004

Klewicki JK, Morgan JJ (1998) Kinetic behavior of Mn(III) complexes of pyrophosphate, EDTA, and citrate. Environ Sci Techmol 32:2916–2922. https://doi.org/10.1021/es980308e

Kostka J, Luther GW, Nealson KH (1995) Chemical and Biological reduction of Mn(III)-pyrophosphate complexes: potential importance of dissolved Mn(III) as an environmental oxidant. Geochim Cosmochim Acta 59:885–894. https://doi.org/10.1016/0016-7037(95)00007-0

Lin H, Taillefert M (2014) Key geochemical factors regulating Mn(IV)-catalyzed anaerobic nitrification in coastal sediments. Geochim Cosmochim Acta 133:17–33. https://doi.org/10.1016/j.gca.2014.01.025

Liu S, Berns A, Vereecken H, Wu D, Brüggemann N (2017) Interactive effects of MnO_2, organic matter and pH on abiotic formation of N_2O from hydroxylamine in artificial soil mixtures. Sci Rep 7:39590. https://doi.org/10.1038/srep39590

Luther GW III (2004) Kinetics of the reactions of water, hydroxide ion and sulfide species with CO_2, OCS and CS_2: frontier molecular orbital considerations. Aquat Geochem 10:81–97. https://doi.org/10.1023/B:AQUA.0000038957.18584.b0

Luther GW III (2005) Manganese(II) oxidation and Mn(IV) reduction in the environment—two one-electron transfer steps versus a single two-electron step. Geomicrobiol J 22:195-203. https://doi.org/10.1080/01490450590946022

Luther GW III (2010) The role of one- and two-electron transfer reactions in forming thermodynamically unstable intermediates as barriers in multi-electron redox reactions. Aquatic Geochem 16:395–420. https://doi.org/10.1007/s10498-009-9082-3

Luther GW III (2016) Inorganic chemistry for geochemistry and environmental sciences: fundamentals and applications. Wiley, Chichester

Luther GW III, Popp JI (2002) Kinetics of the abiotic reduction of polymeric manganese dioxide by nitrite: an anaerobic nitrification reaction. Aquat Geochem 8:15–36. https://doi.org/10.1023/A:1020325604920

Luther GW III, Sundby B, Lewis BL, Brendel PJ, Silverberg N (1997) Interactions of manganese with the nitrogen cycle: alternative pathways to dinitrogen. Geochim Cosmochim Acta 61:4043–4052. https://doi.org/10.1016/S0016-7037(97)00239-1

Luther GW III, Thibault de Chanvalon A, Oldham VE, Estes E, Tebo BM, Madison AS (2018) Reduction of manganese oxides: thermodynamic, kinetic and mechanistic considerations for one- versus two-electron transfer steps. Aquat Geochem 24:257–277. https://doi.org/10.1007/s10498-018-9342-1

Madison AS, Tebo BM, Mucci A, Sundby B, Luther GW III (2013) Abundant Mn(III) in porewaters is a major component of the sedimentary redox system. Science 341:875–878. https://doi.org/10.1126/science.1241396

Matocha CJ, Sparks DL, Amonette JE, Kukkadapu RK (2001) Kinetics and mechanism of birnessite reduction by catechol. Soil Sci Soc Am J 65:58–66. https://doi.org/10.2136/sssaj2001.65158x

Oldham VE, Owings SM, Jones M, Tebo BM, Luther GW III (2015) Evidence for the presence of strong Mn(III)-binding ligands in the water column of the Chesapeake Bay. Mar Chem 171:58–66. https://doi.org/10.1016/j.marchem.2015.02.008

Oldham VE, Jones M, Tebo BM, Luther GW III (2017a) Oxidative and reductive processes contributing to manganese cycling at oxic-anoxic interfaces. Mar Chem 195:122–128. https://doi.org/10.1016/j.marchem.2017.06.002

Oldham VE, Mucci A, Tebo BM, Luther GW III (2017b) Soluble Mn(III)-L complexes are ubiquitous in oxygenated waters and stabilized by humic ligands. Geochim Cosmochim Acta 199:238–246. https://doi.org/10.1016/j.gca.2016.11.043

Oldham VE, Miller MT, Jensen LT, Luther GW III (2017c) Revisiting Mn and Fe removal in humic rich estuaries. Geochim Cosmochim Acta 209:267–283. https://doi.org/10.1016/j.gca.2017.04.001

Owings SM, Luther GW III, Taillefert M (2019) Development of a rate law for arsenite oxidation by manganese oxides. Geochim Cosmochim Acta 250:251–267. https://doi.org/10.1016/j.gca.2019.02.003

Qian A, Zhang W, Shi C, Pan C, Giammar DE, Yuan S, Zhang H, Wang Z (2019) Geochemical stability of dissolved Mn(III) in the presence of pyrophosphate as a model ligand: complexation and disproportionation. Environ Sci Techmol 53:5768–5777. https://doi.org/10.1021/acs.est.9b00498

Siebecker MG, Madison AS, Luther GW III (2015) Reduction kinetics of polymeric (Soluble) manganese (IV) Oxide (MnO_2) by ferrous iron (Fe^{2+}). Aquat Geochem 21(2–4):143–158. https://doi.org/10.1007/s10498-015-9257-z

Stone AT, Morgan JJ (1984a) Reduction and dissolution of manganese (III) and manganese(IV) oxides byorganics. 1. Reaction Hydroquinone Environ Sci Technol 18:450–456

Stone AT, Morgan JJ (1984b) Reduction and dissolution of manganese (III) and manganese(IV) oxides by organics. 2. Survey of the reactivity of organics. Environ Sci Technol 18:617–624

Trouwborst RE, Clement BG, Tebo BM, Glazer B, Luther GW III (2006) Soluble Mn(III) in suboxic zones. Science 313:1955–1957. https://doi.org/10.1126/science.1132876

Watters JI, Kolthoff IM (1948) Potentiometric investigation of tripyrophosphatomanganic (III) acid. J Amer Chem Soc 70:2455–2460

Yakushev E, Pollehne F, Jost F, Kuznetsov I, Schneider B, Umlauf L (2007) Analysis of the water column oxic/anoxic interface in the Black and Baltic seas with a numerical model. Mar Chem 107:388–410. https://doi.org/10.1016/j.marchem.2007.06.003

Yao W, Millero FJ (1993) The rate of sulfide oxidation by δMnO_2 in seawater. Geochim Cosmochim Acta 57:3359–3365. https://doi.org/10.1016/0016-7037(93)90544-7

Yao W, Millero FJ (1995) Oxidation of hydrogen sulfide by Mn(IV) and Fe(III) (hydr)oxides in seawater. In: Vairavamurthy V, Schoonen MAA, Eglinton TI, Luther GW, Manowitz B (eds) Geochemical transformations of sedimentary sulfur. American chemical society symposium series, Washington, pp 260–2799

Zhang X-M, Bordwell FG (1992) Homolytic bond dissociation energies of the benzylic C–H bonds in radical anions and radical cations derived from fluorenes, triphenylmethanes, and related compounds. J Am Chem Soc 114:9787–9792

Zhu-Barker X, Cavazos AR, Ostrom NE, Horwarth WR, Glass JB (2015) The importance of abiotic reactions for nitrous oxide production. Biogeochemistry 126:251–267. https://doi.org/10.1007/s10533-015-0166-4